Available online at www.sciencedirect.com
ScienceDirect
Ceramics International 38 (2012) 731–740
CERAMICS INTERNATIONAL
www.elsevier.com/locate/ceramint

Fabrication of corrosion resistant, bioactive and antibacterial silver substituted hydroxyapatite/titania composite coating on Cp Ti

Venkateswarlu Kotharu[a,b], Rameshbabu Nagumothu[a,*], Chandra Bose Arumugam[b], Muthupandi Veerappan[a], Subramanian Sankaran[c], MubarakAli Davoodbasha[d], Thajuddin Nooruddin[d]

[a] Department of Metallurgical and Materials Engineering, National Institute of Technology, Tiruchirappalli 620 015, Tamilnadu, India
[b] Department of Physics, National Institute of Technology, Tiruchirappalli 620 015, Tamilnadu, India
[c] Department of Materials Engineering, Indian Institute of Science, Bangalore 560 012, Karnataka, India
[d] Department of Microbiology, Bharathidasan University, Tiruchirapalli 620 024, Tamil Nadu, India

Received 18 June 2011; accepted 28 July 2011
Available online 5th August 2011

Abstract

The present work is aimed at developing a bioactive, corrosion resistant and anti bacterial nanostructured silver substituted hydroxyapatite/titania ($AgHA/TiO_2$) composite coating in a single step on commercially pure titanium (Cp Ti) by plasma electrolytic processing (PEP) technique. For this purpose 2.5 wt% silver substituted hydroxyapatite (AgHA) nanoparticles were prepared by microwave processing technique and were characterized by X-ray diffraction (XRD), Fourier-transform infrared (FT-IR) spectroscopy and transmission electron microscopy (TEM) methods. The as-synthesized AgHA particles with particle length ranging from 60 to 70 nm and width ranging from 15 to 20 nm were used for the subsequent development of coating on Cp Ti. The PEP treated Cp Ti showed both titania and AgHA in its coating and exhibited an improved corrosion resistance in 7.4 pH simulated body fluid (SBF) and 4.5 pH osteoclast bioresorbable conditions compared to untreated Cp Ti. The *in vitro* bioactivity test conducted under Kokubo SBF conditions indicated an enhanced apatite forming ability of PEP treated Cp Ti surface compared to that of the untreated Cp Ti. The Kirby–Bauer disc diffusion method or antibiotic sensitivity test conducted with the test organisms of *Escherichia coli* (*E. coli*) for 24 h showed a significant zone of inhibition for PEP treated Cp Ti compared to untreated Cp Ti.

Keywords: A. Microwave processing; B. Nanocomposites; C. Corrosion; E. Biomedical applications

1. Introduction

Titanium and its alloys are widely used for hard tissue replacement, cardiac and cardiovascular devices, owing to their high mechanical strength, low elastic modulus, good corrosion resistance and biocompatibility [1]. However, they exhibit poor bioactivity [2], and consequently it is possible to establish only a mechanical bonding rather than a direct chemical bonding between the titanium implant material and the host bone tissue after implantation. One way to improve the bioactivity of these Ti implant materials is to apply HA coating [3], which has the desirable properties such as biocompatibility, osteoconductivity and bioactivity, on their surface. But, it is difficult for HA coating to chemically bond with Ti at the interface because of their different lattice structures. In addition there is a big difference between their Young's moduli and thermal expansion coefficients [4]. Titanium oxide (TiO_2) coating has attracted considerable attention as a bond coat due to its good *in vivo* corrosion resistance and biocompatibility, apart from its ability to enhance the bonding strength between HA coating and the substrate [5]. Therefore, the development of TiO_2/HA composite coating on Ti with more TiO_2 at the interface and more HA on the outer surface can be envisaged to provide a very good combination of corrosion resistance and bioactivity.

However, the modified Ti implant surface is comparatively rough and is thought to be at a higher risk of bacterial accumulation when exposed to the oral cavity [6]. Thus a serious issue related to these implant devices is the bacterial

* Corresponding author. Tel.: +91 431 2503464; fax: +91 431 2500133.
E-mail addresses: rameshrohith@gmail.com, nrb@nitt.edu (N. Rameshbabu).

0272-8842/$36.00
doi:10.1016/j.ceramint.2011.07.065

infection and it is one of the main causes for recurrent surgery. After adhering onto the implant surface, the bacteria tend to aggregate in a hydrated polymeric matrix to form a biofilm which is the cause of many types of persistent and chronic bacterial infection. Colonization which may occur at the time of surgery or from bacteria from remote sources, where bacteria are seeded at the vicinities of the implants, can lead to acute haematogenous infection [7]. In addition, bacterial infection inducing mucositis or peri-implantitis can destroy dental implants, not only at early osseointegration phases but also the previously well osseointegrated ones [8]. Therefore, an important strategy would be to prevent the initial adhesion of bacteria by making the implant antibacterial.

Keeping in mind the requirements of a successful implant material the present work aims at developing a coating on Cp Ti with significant antibacterial activity and bioactivity as well as better corrosion resistance in biological environments. Additionally, the PEP conditions for developing the coating in a simple single step will be established. Towards this, a composite layer of AgHA/TiO_2 was developed on Cp Ti by PEP, which combines both the plasma electrolytic oxidation (PEO) and electrophoretic deposition (EPD) processes simultaneously.

2. Materials and methods

2.1. Synthesis and characterization of AgHA nanoparticles

As a maximum amount of 2.5 wt% silver can be incorporated in to the HA coating to show significant antibactericidal activity without affecting the bioactivity and without showing osteoblast cell toxicity [9,10], in the present study 2.5 wt% silver substituted HA (here after AgHA) nanoparticles were prepared for the subsequent process of developing the coating. Analytical grade calcium hydroxide [$Ca(OH)_2$, E. Merck, Germany], diammonium hydrogen phosphate [DAP, $(NH_4)_2HPO_4$, E. Merck, Germany] and silver nitrate [$AgNO_3$, E. Merck, Germany], were used for the preparation of AgHA nanoparticles by microwave processing. The advantages of the microwave method of synthesizing HA nanoparticles are reported elsewhere [11,12]. The amount of the reactants was calculated based on the calcium + silver: phosphorus molar ratio of 10:6. The silver nitrate was first dissolved in distilled water (0.25 M solution), and it is added to 0.3 M calcium hydroxide suspension in distilled water under stirring conditions. The 0.3 M DAP solution was added to the silver nitrate dissolved calcium hydroxide aqueous suspension for 5 min under vigorous stirring conditions. Subsequently, the precursor solution in an uncovered glass beaker was immediately subjected to the microwave irradiation for about 30 min in a domestic microwave oven (Samsung India, 2.45 GHz, 850 W power). The crystallization of AgHA and its aging occurred under the microwave irradiation in a short time of about 30 min. Microwave irradiation time was optimized based on the literature [13] and the author's experience in the synthesis of nanosized HA using Ca $(OH)_2$ and DAP as calcium and phosphorus precursors [14]. The precipitate was thoroughly washed with distilled water to remove impurity ions (NH_4^+, NO_3^-). The product obtained after filtration was oven-dried at 90 °C overnight, and the flakes were powdered using an agate mortar and pestle.

The X-ray diffraction pattern was recorded for the as-synthesized AgHA powder particles by using a Rigaku Ultima III X-ray diffractometer with Cu $K\alpha_1$ radiation (λ = 1.54056 Å) over the 2θ range of 20–60°, using a step size of 0.05° and step time of 3 s. The functional groups present in as synthesized AgHA particles were ascertained by Fourier transform infrared spectroscopy (FTIR, Perkin Elmer, Spectrum One, USA) over the region 450–4000 cm^{-1} in pellet form for the powder samples of 1 mg mixed with spectroscopic grade KBr (Merck) of 200 mg. Spectra were recorded at 4 cm^{-1} resolution, averaging 80 scans. The size and morphology of AgHA powder were analyzed by transmission electron microscope (TEM, Philips, CM12 STEM, Netherlands). For TEM analysis, the powder sample was ultrasonically dispersed in ethanol to form a dilute suspension, and then a few drops were deposited on the carbon-coated copper grids.

2.2. Fabrication and characterization of AgHA/TiO_2 composite coating

The AgHA aqueous suspension was prepared by adding 5 g of AgHA powder and 10 ml of ethylene glycol simultaneously to 1 l of distilled water taken in a conical flask. The addition of AgHA powder and ethylene glycol to distilled water was done in several steps and the added contents in the distilled water were hand shaken well at the end of each step to facilitate the effective charging of AgHA. Triethanolamine was used to adjust the pH value of the solution to around 11. The aqueous AgHA suspension was also sonicated using an ultrasonic vibrator [Sonics, 750 W, 20 kHz, USA] for 45 min to obtain a stable dispersion. Finally, 5 g of trisodium ortho phosphate (TSOP, Merck, India) was added to the prepared aqueous AgHA suspension under magnetic stirring conditions. This aqueous AgHA suspended TSOP solution was used as electrolyte for developing AgHA/TiO_2 composite layer by PEP technique.

The Cp Ti test coupons with dimensions of 25 mm × 15 mm × 1.5 mm were abraded down to 1000 grit emery paper and then ultrasonically cleaned in alcohol, acetone and distilled water for 5 min successively before use. Prior to PEP treatment, acid activation was performed for 30 s in a diluted mixture of nitric acid and hydrofluoric acid to remove the natural titanium oxide layer and surface contaminants.

For the PEP treatment, a stainless steel bowl of 15 cm diameter containing the electrolyte system was used as cathode and the specimens were immersed as anode. A DC power supply unit (Milman Thin Films Pvt. Ltd., Pune, India) with a maximum peak voltage of 900 V and a maximum output current of 15 A was employed to carry out the process. The coating process was carried out for 6 min at a constant current of 1.75 A corresponding to a current density of about 200 mA/cm^2 at the work piece. The employed power source was designed so that it could maintain the set constant current value automatically by

adjusting the potential. During the process the electrolyte bath temperature was maintained around 45 °C. To elucidate the coating formation mechanism, specimens treated for 2 min and 4 min were also prepared under the same processing conditions. After the PEP treatment, the specimens treated for 2, 4 and 6 min were cleaned with distilled water and air dried at room temperature. The specimens coated with AgHA/TiO_2 for 6 min were subjected to bioactivity, corrosion and antibacterial testing. In addition, HA/TiO_2 coating was also developed on Cp Ti for 6 min under identical PEP processing conditions to compare the antibacterial action of both pure HA/TiO_2 and AgHA/TiO_2 coatings. The phase composition of the coating was analyzed by Rigaku X-ray diffractometer (Ultima III, Rigaku, Japan) using Cu Kα radiation at 40 kV and 30 mA with a scan speed of 1°/min and a step size of 0.05°. The surface morphology, the coating thickness and the elemental composition of the coating were assessed using a Hitachi-S3000 N scanning electron microscope equipped with energy dispersive spectroscopy facility (EDS).

2.3. Electrochemical corrosion testing under simulated body fluid (SBF) environments

The potentiodynamic polarization and electrochemical impedance spectroscopy (EIS) studies of uncoated and AgHA/TiO_2 coated specimens were carried out at 37 °C under two different pH conditions, one at 4.5 pH simulated osteoclast resorption and another at 7.4 pH simulated body fluid solution. The 4.5 pH condition is responsible for physiological conditions of osteoclast bone resorption [15]. The 4.5 pH test solution was obtained by adding an appropriate amount of nitric acid to distilled water. The 7.4 pH physiological solution for corrosion testing was prepared according to ASTM standard F2129-06. Potentiodynamic polarization and electrochemical impedance spectroscopy (EIS) plots were obtained for both conditions using ACM Gill AC corrosion testing unit to evaluate the corrosion behaviour of Cp Ti before and after PEP treatment. A three electrode cell, with sample as working electrode, saturated calomel electrode (SCE) as reference electrode and platinum foil as counter electrode, was employed in this test. During the anodic polarization scan, the sample with an exposed area of 0.5 cm^2 was kept in contact with the solution and then polarized from cathodic to anodic region at a scan rate of 60 mV/min in the range of −500 mV to 3000 mV with reference to SCE. From the polarization curve, the corrosion current density (I_{corr}) was determined by Tafel extrapolation method using the ACM software provided with the equipment. For EIS studies a small amplitude signal of 10 mV, a frequency range of 10^{-2} Hz to 100 kHz and 50 points per test were employed.

2.4. In vitro bioactivity test

The bioactivity of the fabricated coating was tested by soaking in Kokubo SBF solution prepared as per reported procedure [16]. The SBF solution was refreshed every 24 h. After 10 days of incubation period, the samples were taken out of SBF, rinsed with distilled water, and then dried in an oven at 60 °C for 12 h.

2.5. Antibacterial assessment test

Antibacterial action of both HA/TiO_2 and AgHA/TiO_2 coatings developed for 6 min samples was studied by the disc diffusion test method (commonly known as the Kirby–Bauer disc diffusion method or antibiotic sensitivity test). Mueller–Hinton agar was cast into the petri plates, and the plates containing the nutrient medium were evenly inoculated with the test organisms of *E. coli*. The coated specimens were planted onto the *E. coli* inoculated agar plates separately. These two plates were incubated at 37 °C for 24 h and were examined for a zone of inhibition of bacterial growth around the test specimens.

3. Results and discussion

3.1. Studies on characterization of AgHA nanoparticles

The XRD pattern and FT-IR spectrum of as-synthesized AgHA particles are shown in Fig. 1(a) and (b), respectively. All the diffraction peaks are well matched with the standard JCPDS (9-432) HA with hexagonal crystal structure. As the XRD peaks are markedly broader, indicating that the AgHA particles are nanosized. The average crystallite size in a direction perpendicular to the crystallographic plane was estimated based on Scherrer's formula $D_v = (K\lambda/\beta \cos\theta)$, where D_v is the volume weighted average crystallite size (nm); K is the shape factor ($K \approx 0.9$); λ is the wavelength of the X-rays ($\lambda = 0.154056$ nm for Cu Kα radiation); β is the broadening of the diffraction peak measured at half of its maximum intensity (in radians), and θ is the Bragg's diffraction angle (°). The (0 0 2) diffraction peak at 25.98° was chosen for calculation of the crystallite size along the *c*-axis of the HA crystalline structure. The estimated crystallite size was found to be 31 nm.

The FT-IR spectrum of as-synthesized AgHA exhibits the characteristic bands for HA: 900–1200 cm^{-1} for phosphate bending and stretching, 602 cm^{-1} for phosphate bending, 632 cm^{-1} and 3571 cm^{-1} for vibrational and stretching modes of hydroxyl vibrations. The broadening of the phosphate characteristic bands near 1040 and 1090 cm^{-1} is due to low crystallinity and small dimensional effect of as prepared AgHA particles [17]. The broad absorption band between 3800 and 3000 cm^{-1}, as well as the band at 1652 cm^{-1} corresponds to H_2O adsorbed at the surface. The absorption bands at 873, 1421 and 1455 cm^{-1}, in the as-synthesized AgHA particles corresponding to the presence of carbonate ions, can be attributed to the reaction between carbon dioxide in air and high pH precursor solution [18]. The TEM micrograph of as-synthesized AgHA nanoparticles is shown in Fig. 2. As seen from the micrograph, the particles exhibit needle-like shaped morphology with clear contours and less agglomeration. The particles are found to be nanosized with particle length ranging from 60 to 70 nm and width ranging from 15 to 20 nm. Thus

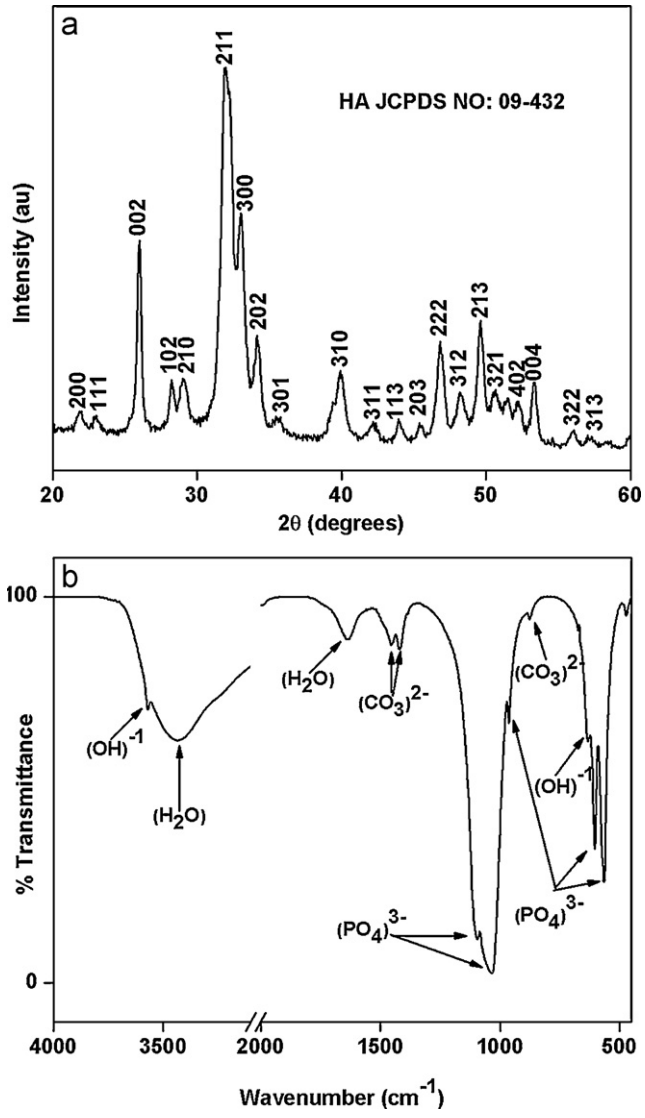

Fig. 1. XRD pattern (a) and FT-IR spectrum (b) of AgHA nanoparticles.

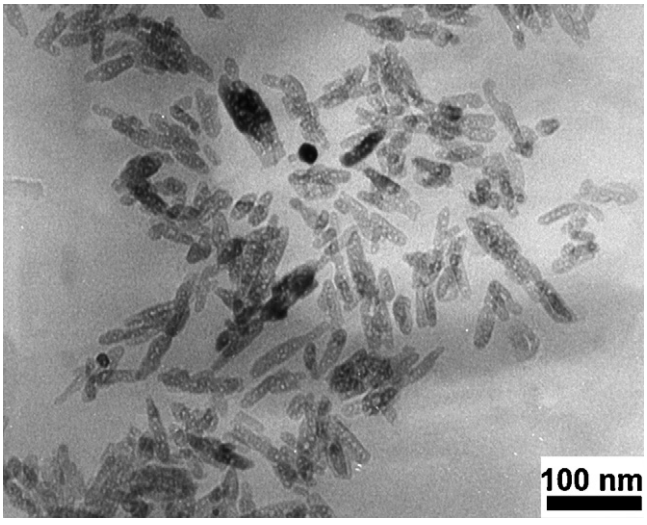

Fig. 2. TEM micrograph of AgHA nanoparticles.

both the XRD and TEM results show that the AgHA particles synthesized by microwave processing are nanosized and have a narrow size distribution. This is because, microwave irradiation of the reaction mixture results in rapid heating, particularly those containing microwave active polar molecules such as water [19]. As a consequence, the precipitation of particles from such solutions tends to be rapid and nearly simultaneous. This leads to very small particle sizes and narrow particle size distributions, in the final products [20].

3.2. Studies on characterization of AgHA/TiO_2 composite coating

The XRD patterns of the samples treated for 2, 4 and 6 min are shown in Fig. 3(a)–(c), respectively. The three XRD patterns show the characteristic intense (2 1 1) diffraction peak at $2\theta \approx 31.6^\circ$ which can be indexed as hexagonal HA phase (JCPDS No: 09-432). The intensity of the intense diffraction peak (2 1 1) of HA is observed to be increasing successively with the PEP treatment time. However there is a drastic increase in the intensity of the (2 1 1) peak of the sample treated for 6 min (Fig. 3(c)) in comparison to that of the sample treated for 4 min (Fig. 3(b)). From this it can be inferred that the incorporation of the suspended AgHA particles in to the developing TiO_2 coating could be accelerated after 4 min of PEP treatment time. This is due to the fact that as the PEP treatment time increases in addition to PEO, electrophoretic deposition also takes place and will result in rapid growth of top AgHA coating which is in support of the proposed brief mechanism in Section 3.5. In addition to HA diffraction peaks, Fig. 3(a)–(c) exhibits the characteristic diffraction peaks of both anatase (at $2\theta \approx 25.3^\circ$, JCPDS No: 21-1272) and rutile (at $2\theta \approx 27.7^\circ$, JCPDS No: 21-1276) TiO_2. Thus Fig. 3 confirms the presence of both TiO_2 and AgHA phases in the coating. As the process was carried out at high anodic potentials and in an electrolyte system composed of low TSOP concentration, the possibility of diffusion of the PO_4^{3-} anionic species from the

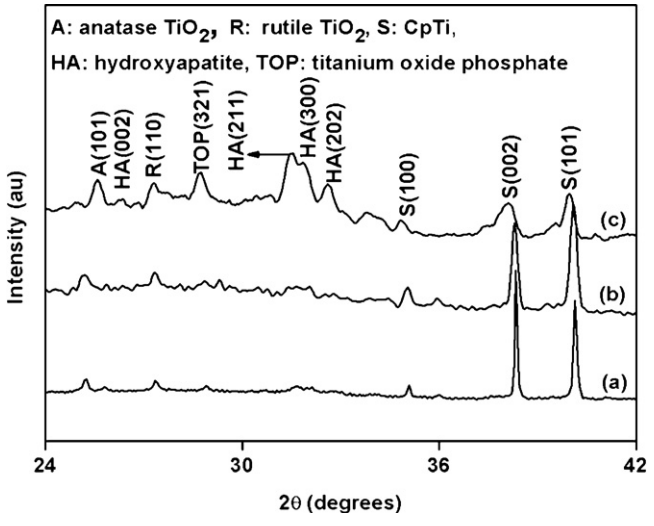

Fig. 3. XRD patterns of PEP treated Cp Ti (a) for 2 min, (b) for 4 min and (c) for 6 min.

electrolyte in to the coating exists, thereby forming a complex phase of titanium oxide phosphate [$Ti_5O_4(PO_4)_4$] observed at $2\theta \approx 28^\circ$ (JCPDS No: 82-1340) in Fig. 3. However, as it is non-toxic it may not show any adverse effect on the bioactivity of the coating. The XRD results did not show characteristic peaks of any other calcium phosphate indicating that there is no phase transition or decomposition of the AgHA in the coating.

The SEM micrographs of the surface of the Cp Ti treated for 2 min and 6 min are shown in Fig. 4(a) and (b), respectively. It is evident that the sample treated for 2 min contains uniformly distributed dark circular spots which are discharge channels open to the surface of the coating. The size of these pores or discharge channels is observed to be 2–4 μm. In addition to the fine AgHA particles adhered and well distributed on the surface of the grown TiO_2 layer, a few agglomerates of AgHA particles trapped in to the pores (which are shown in black circles) can also be seen in Fig. 4(a). Fig. 4(b) shows the AgHA/TiO_2 coating on the substrate. It can be inferred from Fig. 4(a) that the formation of TiO_2 takes place initially under low anodic potentials. The coating developed for 6 min is relatively free of pores due to the AgHA/TiO_2 composite layer formation in comparison to the formation of only TiO_2 after 2 min. The cross sectional morphology of the coating developed for 6 min is shown in Fig. 4(c). The coating exhibits uniformity and is adherent with a thickness of 83 ± 3 μm. The substrate, substrate–coating interface, AgHA/TiO_2 composite layer could be distinctly observed.

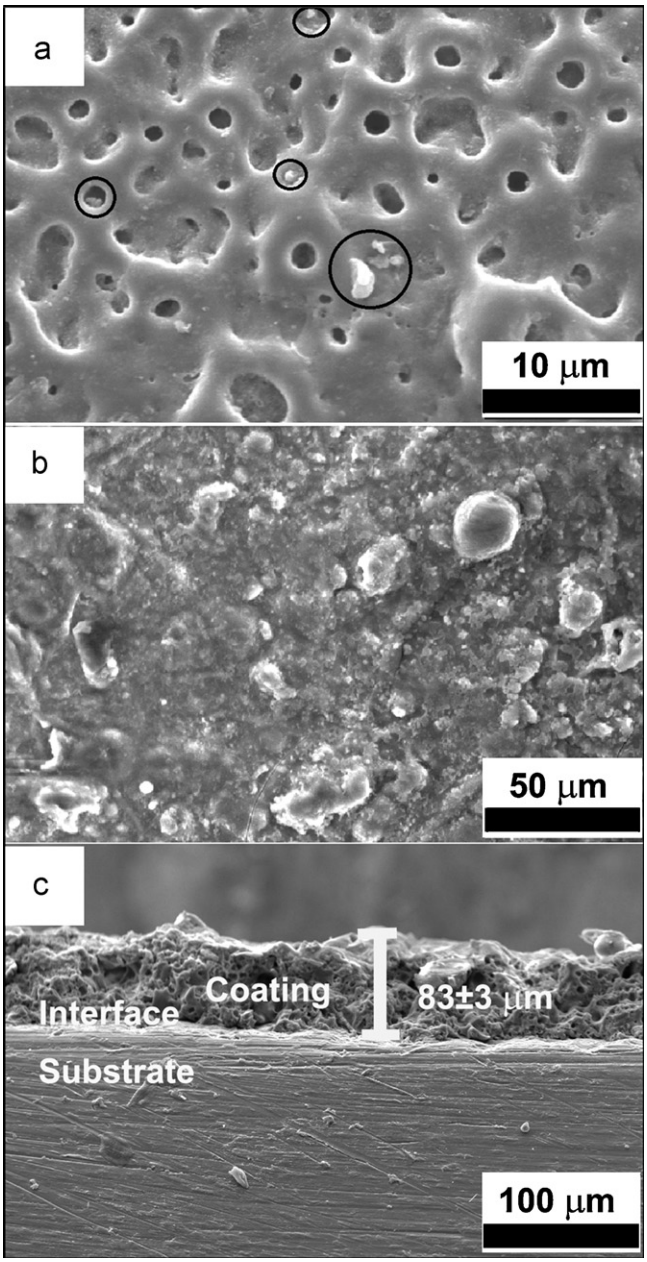

Fig. 4. SEM micrographs of PEP treated Cp Ti (a) for 2 min, (b) for 6 min and (c) SEM cross-sectional micrograph of PEP treated for 6 min.

The energy dispersive X-ray (EDX) spectra of samples treated for 2, 4 and 6 min are shown in Fig. 5(a)–(c), respectively. The Ag counts in the figure confirm the incorporation of Ag in HA. The coating developed for 2 min possesses comparatively a high content of Ti (Fig. 5(a)) indicative of the dominant formation of TiO_2 in the initial stage of the process. Fig. 5(b) shows nearly equal intensities of Ti, Ca and P attesting to the formation of AgHA/TiO_2 composite in the near middle stage of the process. The very low intensity of Ti and the higher intensities of Ca and P (Fig. 5(c)) in the coating developed for 6 min indicate the predominance of AgHA during the final stage of the process. Thus the XRD and EDX results confirm the dominance of PEO in the initial stages and the dominance of EPD in the final stages of the PEP that was carried out in a single step, whereas Nie et al. [21] developed a 30 μm thick pure HA/TiO_2 coating on Ti–6Al–4V with HA as the top layer and TiO_2 as an inner layer by a two step process employing micro discharge oxidation (MDO) and EPD one after the other with two separate electrolyte systems.

3.3. Electrochemical corrosion studies under simulated body fluid (SBF) environments

The cyclic potentiodynamic polarization curves for untreated and PEP treated (6 min) Cp Ti samples in 4.5 and 7.4 pH corrosion media are shown in Fig. 6. The polarization curves obtained from the tests done in 4.5 pH medium show that the untreated Cp Ti remains passive up to 1200 mV and then shows a linear increase of corrosion current density at higher sweep potentials whereas the PEP treated sample nearly remains passive over the entire range of test potential. In addition, the PEP treated sample shows a significant increase in the corrosion potential (E_{corr}), linear polarization resistance (R_p) and a decrease in the corrosion current density (I_{corr}). The E_{corr}, I_{corr}, as well as the anodic and cathodic Tafel slopes (b_a and b_c, respectively) are obtained from the potentiodynamic polarization curves using the Tafel least-squares fitting method. The polarization resistance (R_p) is calculated using the Stern–Geary equation given as $R_p = [b_a b_c / 2.303 I_{corr}(b_a + b_c)]$ [22]. The values of the corrosion parameters obtained from polarization curves using Tafel least square fitting method are shown in Table 1.

It could be seen from Table 1 that the corrosion current density and corrosion rate of treated specimen are significantly

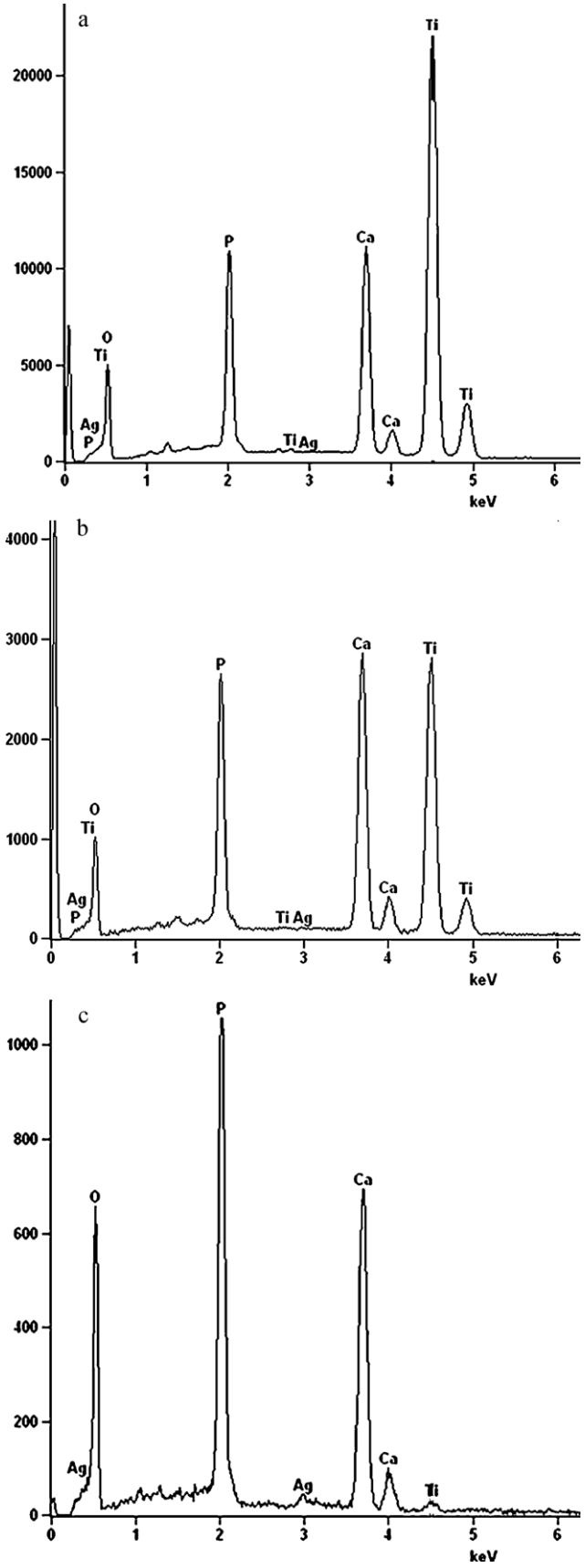

Fig. 5. EDS spectra of PEP treated Cp Ti (a) for 2 min, (b) for 4 min and (c) for 6 min.

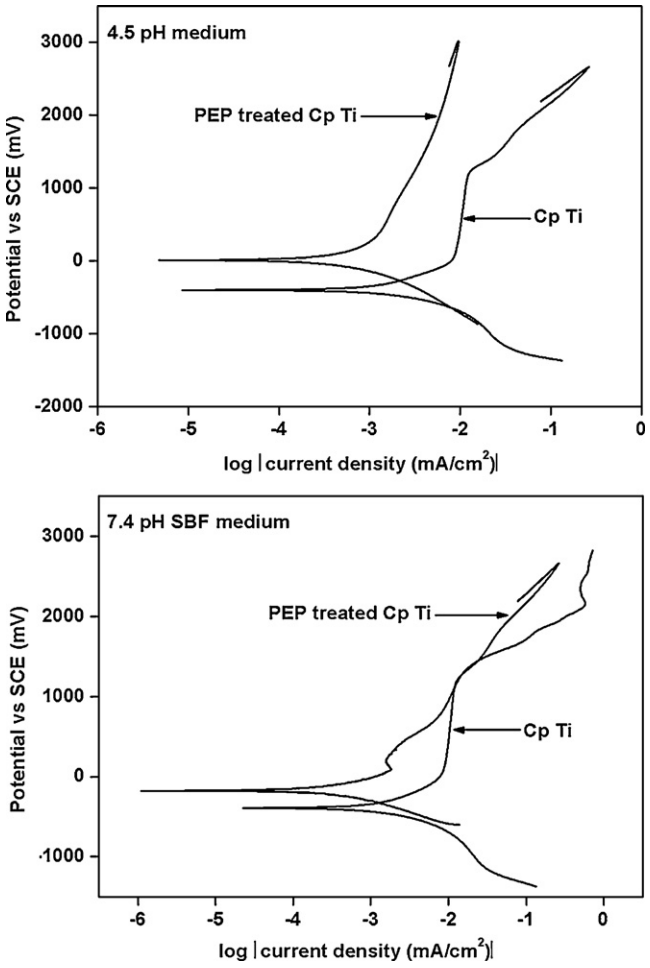

Fig. 6. Potentiodynamic polarization curves of Cp Ti and PEP treated for 6 min in 4.5 and 7.4 pH biological conditions.

lesser than that of untreated specimen under simulated osteoclast resorption condition of 4.5 pH. The improved corrosion resistance was also evidenced by the higher linear polarization resistance (LPR) of treated specimen than that of untreated sample. Similarly, the corrosion resistance of the treated specimen was improved in 7.4 pH Hank's solution medium. However, the corrosion resistance of both treated and untreated specimens in 7.4 pH medium was lesser than the more severe 4.5 pH medium. This may be attributed to the presence of highly corrosive Cl^- ions in 7.4 pH Hank's SBF medium. In agreement with these observations, it has been reported that corrosion is associated with the penetration of chloride ion and water into the coating, transport of ions through the coating, and the subsequent electrochemical reactions at the interface of barrier coating and substrate [23]. Thus in contradiction to the pH of the medium, the PEP treated specimen shows relatively better corrosion resistance in 4.5 pH medium compared to that in 7.4 pH medium. However, the significant improvement in the corrosion resistance of the treated specimens in both 4.5 and 7.4 pH conditions is due to the fact that the $AgHA/TiO_2$ layer acts as a barrier to the transport of electrons and ions between the substrate and the electrolyte, thus reducing the electrochemical reaction rate. The improved corrosion resistance of the coated

Table 1
The corrosion parameter values determined for untreated and PEP treated Cp Ti.

Corrosion parameter	4.5 pH corrosion medium		7.4 pH corrosion medium	
	Cp Ti	PEP treated	Cp Ti	PEP treated
Rest potential (mV)	−169.54	138.03	−362.52	439.21
I_{corr} (mA/cm^2) $\times 10^{-3}$	0.188	0.088	2.04	1.96
LPR (ohm cm^2)	138,730	295,990	12,778	13,255
Corrosion rate (mm/year) $\times 10^{-2}$	0.32	0.10	3.54	3.42

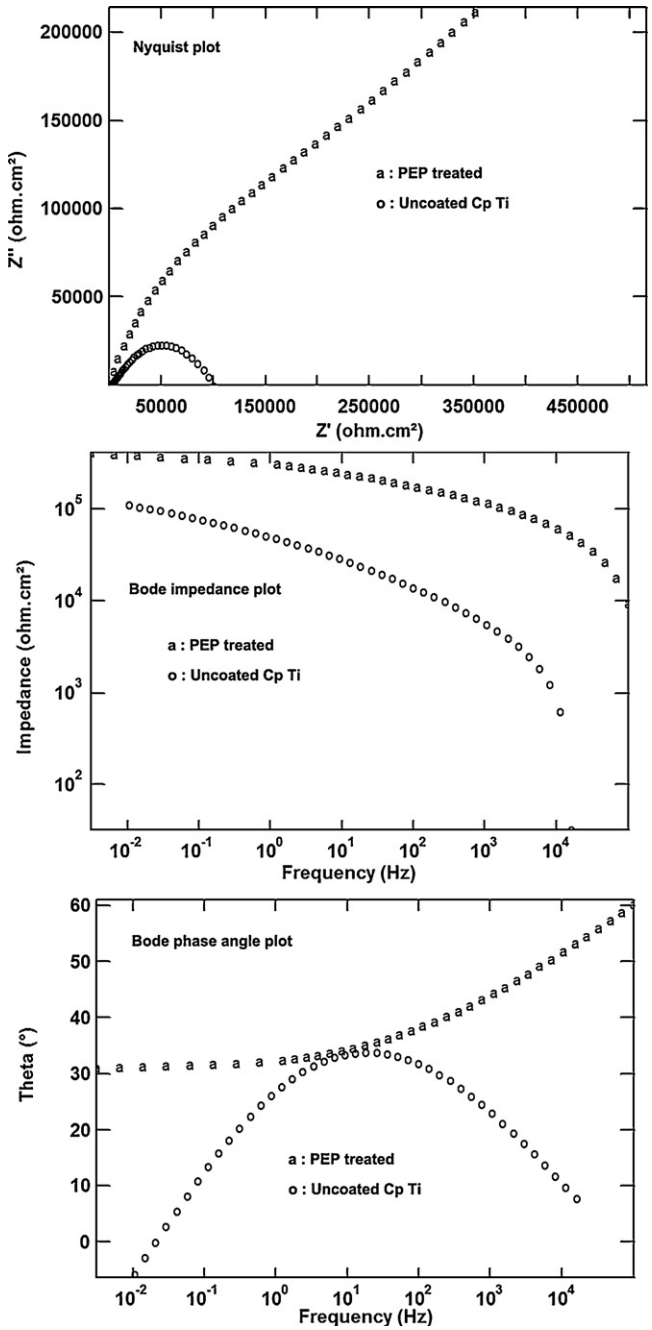

Fig. 7. Nyquist and Bode plots for uncoated and PEP treated Cp Ti in 7.4 pH biological condition.

Cp Ti is ascribed to the combined effect of the semi-insulating TiO_2–AgHA phases in the composite coating.

The Nyquist and Bode impedance, phase angle plots of EIS data obtained from tests done at 7.4 pH condition for uncoated and PEP treated specimens are shown in Fig. 7. For uncoated Cp Ti the polarization resistance is shown to be 9.82×10^4 ohm cm^2 and the total impedance value shown is of the order of 10^4 ohm cm^2. The coated sample showed comparatively a higher polarization resistance value (1.21×10^6 ohm cm^2) and a higher (of the order of 10^5) total impedance value. As shown in the Bode impedance plot of Fig. 7, the coated specimen has comparatively a higher impedance value at a lower frequency which is in good agreement with the well known fact that specimens that show a high impedance value at lower frequency exhibits a better corrosion resistance [24]. As shown in the Bode phase angle plot of Fig. 7, the impedance spectrum of the uncoated Cp Ti reveals a phase angle close to 33° over a shorter range of frequencies, in contrast to the spectrum of the coated Cp Ti that shows a phase angle close to 62° over the wide range of frequencies. It is well known that pure capacitor behaviour is plotted as a positive value of 90° [24]. As the phase angle of coated Cp Ti is comparatively closer to 90°, its response is nearer to pure capacitive which indicates that the coating can reduce the corrosion rate of Cp Ti in the 7.4 pH biological condition. These results are complementary to those obtained from the potentiodynamic polarization curves shown in Fig. 6. Similar trend was also observed with the results obtained from the tests done in 4.5 pH condition. Thus the increase in the polarization resistance and the total impedance value of PEP treated specimen is indicative of increased

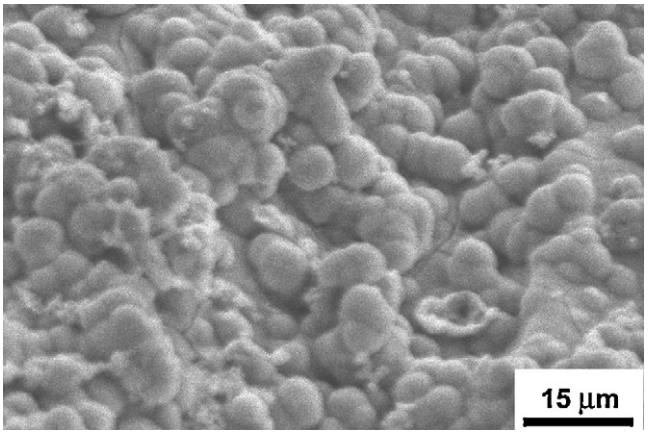

Fig. 8. SEM micrograph of 6 min PEP treated Cp Ti soaked for 10 days in SBF at 37 °C.

corrosion resistance of the Ag HA/TiO_2 composite coating fabricated on Cp Ti.

3.4. Antibacterial assessment studies

The scanning electron micrograph of the treated Cp Ti after the *in vitro* bioactivity test result is shown in Fig. 8. From the surface morphology of the PEP treated Cp Ti immersed in Kokubo's SBF solution for 10 days, it is observed that the surface of the treated specimen is almost fully covered by a newly formed HA layer indicating its improved bioactivity.

The antibiotic susceptibility test result of HA/TiO_2 and Ag HA/TiO_2 coated specimens are shown in Fig. 9(a) and (b), respectively. The petri plates, uncoated portion of the test specimens and the antibacterial zone of inhibition are labelled by p, c and d, respectively. A colour contrast between the pure HA/TiO_2 (Fig. 9(a)) and Ag HA/TiO_2 (Fig. 9(b)) coated specimens could be observed because of the Ag substitution in HA. Ag HA/TiO_2 (Fig. 9(b)) coated specimen appears comparatively yellowish in colour. The direct effect of silver ions leaching out of the Ag HA/TiO_2 coated specimen in the culture medium could result in the formation of a zone of bacterial inhibition which is dark grey in colour and is indicated by 'd' in Fig. 9(b). The presence of zone of bacterial inhibition around the AgHA/TiO_2 coated specimen (Fig. 9(b)) provides the evidence for the bacteriostatic effect of the silver substituted HA in the coating. However the HA/TiO_2 coated and the uncoated portions of the test specimens have not shown any zone of bacterial inhibition. Thus AgHA/TiO_2 composite coated Cp Ti with antibacterial property and bioactivity seems to be a potential material for orthopaedic and dental applications.

3.5. Mechanism of AgHA/TiO_2 composite coating formation

In the present investigation, plasma electrolytic processing was carried out in constant current mode for different time periods to understand the mechanism of formation of AgHA/TiO_2 composite layer. The electrolyte system for this process consists of both oxidizing electrolyte ($Na_3PO_4{\cdot}12H_2O$) and AgHA suspension. In constant current mode of PEP, based on the exposure area (S) of the test specimen and a suitable current density (j), a current ($i = j \times S$) value is set initially. During the initial stage of the process, when the potential is applied, the OH^- ions in the electrolyte tend to move to the anodic surface (Cp Ti) and take part in the following reaction to form an oxide layer.

$$Ti^{4+} + 2OH^- + 2H_2O \rightarrow TiO_2 + 2H_3O^+ + 4e^- \quad (1)$$

As the oxide layer grows in thickness, higher voltages need to be applied to reach the dielectric breakdown of the already grown oxide layer and thereby allowing further anodic reaction to take place. Therefore as the potential continues to increase to maintain the constant current value, the process persists for longer duration.

Under the higher applied anodic potentials the incorporation of charged AgHA [$Ca_{9.7}Ag_{0.3}(PO_4)_6(O^-)_2$] particles in to the growing oxide layer takes place by EPD along with OH^- ions simultaneously. The EPD process consists of the movement of electrically charged particles under the influence of an electric field applied to a stable colloidal suspension and the subsequent deposition on the substrate. The electrophoretic velocity (v) of the suspended AgHA particles can be related to the applied voltage and the apparent particle radius (r) by the relation $v = QE/4\pi r\eta$ [25], where Q stands for surface charge of the particles, E is the potential difference applied to the particle suspension to generate the electric field and η is the viscosity of the particle suspension. As the change in the concentration of suspension solution is negligible and as the temperature of the suspension solution is maintained around 45 °C during the process the viscosity η of the aqueous AgHA suspension can be considered as constant throughout the process. So from the expression for v, it can be seen that the electrophoretic velocity mainly depends on the surface charge of the AgHA particles, intensity of electric field and particle size. Hence, particles with

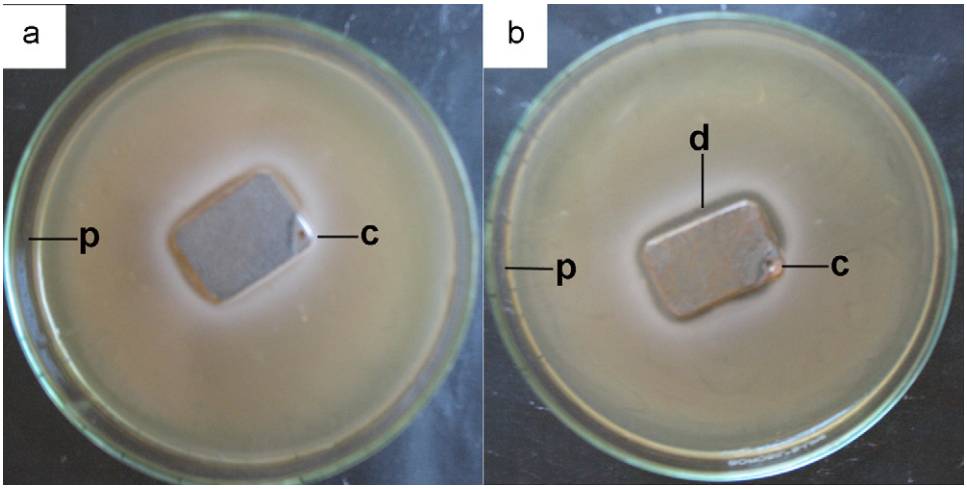

Fig. 9. Kirby–Bauer disk diffusion test result (a) of TiO_2/HA and (b) of TiO_2/AgHA coated Cp Ti treated for 6 min. p, petri plates; c, uncoated portion of Cp Ti; d, zone of bacterial inhibition.

smaller size will have higher electrophoretic velocities even at lower potentials and thus will be incorporated in to the growing oxide layer. As shown in Fig. 2, the microwave synthesized AgHA particles have a narrow range of size distribution (60–70 nm length and 15–20 nm width). Therefore, lesser number of AgHA particles from the suspension solution would have been incorporated in to the growing oxide layer at a lower potential of 280 V observed at the end of 2 min of processing time as shown in Fig. 4(a). This can be further evidenced by the smaller intensity of (2 1 1) diffraction peak in Fig. 3(a). Furthermore, when the specimen treated for 4 min is considered, more amount of AgHA particles have incorporated into the coating as evidenced by Fig. 3(b). This can be attributed to the final potential of 345 V at the end of 4 min. With the increase in the potential, more number of AgHA particles gain higher electrophoretic velocities and will be drifted towards the coating. Similarly, further increase in treatment time to 6 min, at which the final potential reached 415 V, much improvement in the intensity of the (2 1 1) diffraction peak in Fig. 3(c) can be observed. Thus as the potential increases with the processing time (or with the thickness of the coating), the AgHA particles that attain different electrophoretic velocities will be incorporated in to the coating accordingly. Hence the incorporation of the AgHA suspended particles into the oxide layer continues with the increase in applied potential. It is worthwhile to note that the incorporation of AgHA particles into the coating occurs rapidly at the higher potentials as evident by comparing the XRD patterns shown in Fig. 3(b) and (c). Thus, as the PEP processing time increases the tendency of electrophoretic deposition seems to be dominant than plasma electrolytic oxidation. Due to this, more $Ca_{9.7}Ag_{0.3}(PO_4)_6(O^-)_2$ will migrate to the anodic surface and will be sintered by the plasma arc discharges. The characteristic pores of PEO observed after 2 min of processing (Fig. 4(a)) and a comparatively less porous morphology observed after 6 min (Fig. 4(b)) suggest that the TiO_2 formation seems to be a dominant activity during the initial stages of processing, whereas AgHA deposition becomes dominant at the later stages of processing. This has been confirmed by the EDX results shown in Fig. 5. Hence, the fabrication of AgHA/TiO_2 composite coating on Cp Ti takes place by both PEO and EPD simultaneously during the PEP treatment.

4. Conclusions

AgHA/TiO_2 nanocomposite layer was developed on Cp Ti by a single step process called plasma electrolytic processing which is a combination of PEO and EPD techniques. Relatively thick, 83 ± 3 μm, AgHA/TiO_2 layer was developed by the process within 6 min. The results of the corrosion tests under physiological conditions showed a significant improvement in the corrosion resistance and an added capacitive nature for the AgHA/TiO_2 coated Cp Ti implant material compared to that of the uncoated. Besides an improvement in corrosion resistance and bioactivity, the AgHA/TiO_2 composite layer also showed a significant bactericidal effect thus opening up a new class of Ti implants for orthopaedic and dental applications.

Acknowledgements

The authors would like to acknowledge the grant from the Department of Biotechnology, New Delhi (BT/PR-11731/MED/32/99/2008, dated 19-08-2009) and the collaborative research project sanctioned by UGC-Networking Resource Centre for Materials, Department of Materials Engineering, Indian Institute of Science, Bangalore.

References

[1] X.J. Tao, S.J. Li, C.Y. Zheng, J. Fu, Z. Guo, Y.L. Hao, R. Yang, Z.X. Guo, Synthesis of a porous oxide layer on a multifunctional biomedical titanium by micro-arc oxidation, Mater. Sci. Eng. C 29 (2009) 1923–1934.
[2] D. Wei, Y. Zhou, C. Yang, Characteristic, cell response and apatite-induction ability of microarc oxidized TiO_2-based coating containing P on Ti6Al4V before and after chemical-treatment and dehydration, Ceram. Int. 35 (2009) 2545–2554.
[3] D. Wei, Y. Zhou, Preparation, biomimetic apatite induction and osteoblast proliferation test of TiO_2-based coatings containing P with a graded structure, Ceram. Int. 35 (2009) 2343–2350.
[4] J.Y. Han, Z.T. Yu, L. Zhou, Hydroxyapatite/titania composite bioactive coating processed by sol–gel method, Appl. Surf. Sci. 255 (2008) 455–458.
[5] D. Qiu, L. Yang, Y. Yin, A. Wang, Preparation and characterization of hydroxyapatite/titania composite coating on NiTi alloy by electrochemical deposition, Surf. Coat. Technol. 205 (2011) 3280–3284.
[6] M. Esposito, J.M. Hirsch, U. Lekholm, P. Thomsen, Biological factors contributing to failures of osseointegrated oral implants. (II). Etiopathogenesis, Eur. J. Oral Sci. 106 (1998) 721–764.
[7] H. Cao, X. Liu, F. Meng, P.K. Chu, Biological actions of silver nanoparticles embedded in titanium controlled by micro-galvanic effects, Biomaterials 32 (2011) 693–705.
[8] T. Berglundh, L. Persson, B. Klinge, A systematic review of the incidence of biological and technical complications in implant dentistry reported in prospective longitudinal studies of at least 5 years, J. Clin. Periodontol. 29 (2002) 197–212.
[9] M. Bellatone, H.D. Williams, L.L. Hench, Broad-spectrum bactericidal activity of Ag_2O-doped bioactive glass, Antimicrob. Agents Chemother. 46 (2002) 1940–1945.
[10] W. Chen, Y. Liu, H.S. Courtney, M. Bettenga, C.M. Agrawal, J.D. Bumgardner, J.L. Ong, In vitro anti-bacterial and biological properties of magnetron co-sputtered silver-containing hydroxyapatite coating, Biomaterials 27 (2006) 5512–5517.
[11] N. Rameshbabu, T.S. Sampath Kumar, T.G. Prabhakar, V.S. Sastry, K.V.G.K. Murty, K. Prasad Rao, Antibacterial nanosized silver substituted hydroxyapatite: synthesis and characterization, J. Biomed. Mater. Res. A 80 (3) (2007) 581–591.
[12] S.J. Kalita, S. Verma, Nanocrystalline hydroxyapatite bioceramic using microwave radiation: synthesis and characterization, Mater. Sci. Eng. C 30 (2010) 295–303.
[13] B. Vaidhyanathan, K.J. Rao, Rapid microwave assisted synthesis of hydroxyapatite, Bull. Mater. Sci. 19 (1996) 1163–1165.
[14] N. Rameshbabu, K.P. Rao, T.S.S. Kumar, Accelerated microwave processing of nanocrystalline hydroxyapatite, J. Mater. Sci. 40 (2005) 6319–6323.
[15] D. Tadic, F. Peters, M. Epple, Continuous synthesis of amorphous carbonated apatites, Biomaterials 23 (2002) 2553–2559.
[16] T. Kokubo, H. Takadama, How useful is SBF in predicting in vivo bone bioactivity? Biomaterials 27 (2006) 2907–2915.
[17] Y. Zhang, L. Zhou, D. Li, N. Xue, X. Xu, J. Li, Oriented nanostructured hydroxyapatite from the template, Chem. Phys. Lett. 376 (2003) 493–497.
[18] P.N. Kumta, C. Sfeir, D.H. Lee, D. Olton, D. Choi, Nanostructured calcium phosphates for biomedical applications: novel synthesis and characterization, Acta Biomater. 1 (2005) 65–83.

[19] A. Lew, P.O. Krutzik, M.E. Hart, A.R. Chamberlin, Increasing rates of reaction: microwave-assisted organic synthesis for combinatorial chemistry, J. Comb. Chem. 4 (2002) 95–105.
[20] B.L. Cushing, V.L. Kolesnichenko, C.J. Connor, Recent advances in the liquid-phase syntheses of inorganic nanoparticles, Chem. Rev. 104 (2004) 3893–3946.
[21] X. Nie, A. Leyland, A. Matthews, Deposition of layered bioceramic hydroxyapatite/TiO_2 coatings on titanium alloys using a hybrid technique of micro-arc oxidation and electrophoresis, Surf. Coat. Technol. 125 (2000) 407–414.
[22] M. Stern, A.L. Geary, Electrochemical polarization. I. A theoretical analysis of the shape of polarization curves, J. Electrochem. Soc. 104 (1957) 56–63.
[23] C.T. Kwok, P.K. Wong, F.T. Cheng, H.C. Man, Characterization and corrosion behavior of hydroxyapatite coatings on Ti6Al4V fabricated by electrophoretic deposition, Appl. Surf. Sci. 255 (2009) 6736.
[24] D. Qiu, L. Yang, Y. Yin, A. Wang, Preperation and characterization of hydroxyapatite/titania composite coating on NiTi alloy by electrochemical deposition, Surf. Coat. Technol. 205 (2011) 3280–3284.
[25] P.M. Cortez, G.V. Gutierrez, Electrophoretic deposition of hydroxyapatite submicron particles at high voltages, Mater. Lett. 58 (2004) 1336–1339.